Hindawi
Journal of Nanomaterials
Volume 2018, Article ID 9061378, 7 pages
https://doi.org/10.1155/2018/9061378

*Research Article*

# Synthesis of $\alpha$-Alumina Nano-Onions by Thermal Decomposition of Aluminum Formate

**Nadia Vargas-Martínez,[1] Álvaro de Jesús Ruíz-Baltazar,[2] Nahúm A. Medellín-Castillo,[3] and Simón Yobanny Reyes-López[1]**

[1]*Instituto de Ciencias Biomédicas, Envolvente del PRONAF y Estocolmo s/n, Universidad Autónoma de Ciudad Juárez, 32300 Ciudad Juárez, CHIH, Mexico*
[2]*CONACYT-Centro de Física Aplicada y Tecnología Avanzada, Boulevard Juriquilla 3001, 76230 Santiago de Querétaro, QRO, Mexico*
[3]*Centro de Investigación y Estudios de Posgrado, Facultad de Ciencias Químicas, Av. Dr. M. Nava No. 6, Universidad Autónoma de San Luis Potosí, 78210 San Luis Potosí, SLP, Mexico*

Correspondence should be addressed to Álvaro de Jesús Ruíz-Baltazar; alvarodejesusruiz@yahoo.com.mx
and Simón Yobanny Reyes-López; simon.reyes@uacj.mx

Received 26 December 2017; Revised 22 March 2018; Accepted 8 May 2018; Published 2 July 2018

Academic Editor: Ping Xiao



A simplified route to prepare $\alpha$-$Al_2O_3$ nano-onions and alumina powders with an excellent surface area through the thermal decomposition of aluminum formate ($Al(O_2CH)_3$) precursor is proposed. The calcined powders were characterized by infrared and $^{13}C$ MAS NMR spectroscopy. Coordination numbers and chemical interactions were determined by $^{27}Al$ MAS NMR spectroscopy. The $^{27}Al$ MAS NMR spectra showed the presence of $\eta$-$Al_2O_3$ at 1000°C, and the transformation to $\alpha$-$Al_2O_3$ at 1100°C. The spectral data also showed that while the precursor contained 6-coordinated aluminum ions, four-, five-, and six-coordinated aluminum species were present after calcination at 400°C. SEM images and BET measurements of $\alpha$-$Al_2O_3$ revealed aggregated particles with a specific surface area of 118 $m^2/g$. A nano-onion structure of $\alpha$-$Al_2O_3$ was evident from the HRTEM image.

## 1. Introduction

Aluminum oxide, also known as alumina, is one of the most important oxides used industrially. Alumina can be found in several metastable transition phases, determined by the temperature and precursor employed to obtain the oxide. Phase transition in alumina follows the sequence $\gamma$-$Al_2O_3 \rightarrow \delta$-$Al_2O_3 \rightarrow \theta$-$Al_2O_3 \rightarrow \alpha$-$Al_2O_3$ [1]. Each of the phases presents characteristic properties that allow this ceramic to be used for diverse applications such as reinforcement, catalysts, refractories, and adsorbents [2]. The most stable and widely utilized alumina phase is the alpha phase. $\alpha$-$Al_2O_3$ is used as an advanced ceramic given its high chemical stability, hardness, high refractoriness, high thermal conductivity, good wear resistance, and electrical insulation [3]. Some applications include fabrication of reinforcers, electronics, photonics, sensors, and catalysts [4].

The properties of $\alpha$-$Al_2O_3$ are enhanced when its particle size reaches the nanoscale [5], resulting in a large surface area. Manipulation of matter at this scale makes it possible to exploit the best characteristics of the material and to eliminate the properties that reduce its potential. Many methods such as combustion, precipitation, mechanical milling, addition of seeding materials, synthesis of nanoclusters, vapor-phase reaction, liquid-solid-phase synthesis, and hydrothermal synthesis have been used to obtain $\alpha$-$Al_2O_3$ powders. However, most of these methods employ aluminum hydrates and have their own disadvantages [6, 7].

The challenge in the preparation of nano-$\alpha$-$Al_2O_3$ powders resides on the high temperature required for the

transition of $\gamma$-$Al_2O_3$ and/or $\theta$-$Al_2O_3$ to $\alpha$-$Al_2O_3$. High temperatures (>1200°C) are required to overcome the activation energy barrier and induce transformation; nevertheless, such high temperatures can also induce rapid grain growth or agglomeration of alumina particles, thus impeding the formation of nanoparticles [8]. For this reason, the synthesis of $\alpha$-$Al_2O_3$ at low temperatures has been studied.

Although the sequence of phase transformation of aluminum hydroxides has been well described [9], the formation of alumina from metalorganic compounds such as aluminum formate has not been completely studied. Characterization of thermal decomposition behavior can demonstrate the phase transformation process and help determine the optimum conditions for the process and the temperatures where the phases appear. Additionally, the formation of $(Al_2O_3)_n$ nanoclusters can be demonstrated. The chemical or physical properties of alumina nanoclusters can be exploited for hydrogen storage. Hydrogen is an important energy carrier, exerting low environmental impact, that could be used as a sustainable energy source. Currently, efficient hydrogen storage materials constitute an important subject in material research [10].

Characterization by $^{13}C$ MAS NMR, $^{27}Al$ MAS NMR, Fourier transform infrared (FT-IR) spectroscopy, and scanning electron microscopy showed the thermal transformation of aluminum formate to $\alpha$-$Al_2O_3$ at low temperatures. HRTEM results demonstrated the formation of alumina nano-onions by simple decomposition of aluminum formate.

## 2. Methods

Aluminum formate, $Al(O_2CH)_3$, was synthetized using the method established by Reyes-López et al. [11], wherein aluminum and formic acid produced aluminum formate at room temperature. This solution was then spray dried in order to obtain fine powders. The route for the synthesis of $\alpha$-alumina nano-onions involves the dissolution of the precursor aluminum formate in water using a magnetic stirrer. After it, the final solution was keeping stirred until it was heated to obtain a white gel. This gel was transferred to a closed platinum crucible to put in a furnace up to 1100°C at a rate of 5 K·minute$^{-1}$, obtaining a blackish voluminous fluffy solid product while the oxygen-depleted atmosphere is controlled to prevent the oxidation. Finally, this product was calcined at 900°C for 2 h to form a white powder.

The precursor powders were heat treated at 80, 240, 270, 400, 900, 1050, and 1100°C in a Thermolyne furnace in order to observe the transformation of aluminum formate to $\alpha$-$Al_2O_3$.

Aluminum formate and alumina powders were characterized by FT-IR, $^{13}C$ and $^{27}Al$ MAS NMR spectroscopy, scanning electron microscopy (SEM), Brunauer-Emmett-Teller (BET) surface area analysis, scanning transmission electron microscopy (STEM), and high-resolution transmission electron microscopy (HRTEM). FT-IR analysis was performed using Bruker PLATINUM ATR equipment with the following settings: diamond crystal, 32 scans, resolution of 4 cm$^{-1}$, and cumulative scan from 400 to 4000 cm$^{-1}$. The solid-state evolution of the precursor was characterized by $^{13}C$ and $^{27}Al$ MAS NMR at 22°C under the following conditions: $\pi/2 = 2.0\,\mu$s pulse, relaxation time of 60 s, and sample spinning at 14 kHz for $^{27}Al$ MAS; $\pi/2 = 5.0\,\mu$s pulse, relaxation time of 60 s, and sample spinning at 10 kHz for $^{13}C$ MAS. The spectra were referenced using 1.0 M $Al(NO_3)_3$ solution, adamantine, and $H_2O$ for $^{27}Al$ MAS (0.0 ppm) and $^{13}C$ MAS (38.48 ppm). SEM images were obtained using Jeol JSM-6400 at 15 kV. The specific surface area of the calcined samples was determined by nitrogen sorption according to the single-point BET method using a Quantachrome apparatus. STEM and HRTEM observations were performed using Philips TECNAI 20 Super Twin at 200 kV.

## 3. Results and Discussion

Aluminum formate was obtained as part of a white solution along with aluminum fragments. After subjecting the solution to spray drying, high-purity aluminum formate was produced. Figure 1 shows the IR spectrum of aluminum formate thermally decomposed under the mentioned temperatures. At 25°C, the compound showed vibrations within the range of 3300–2500 cm$^{-1}$ due to the structural OH group, while symmetric deformation vibrations observed at 2927 and 1094 cm$^{-1}$ indicated the presence of C-H bonds in the molecule. Bands, representing asymmetric COC stretching and deformation vibrations, and symmetric COC stretching and deformation vibrations in the regions 1620, 1400, 1375, and 800 cm$^{-1}$ were attributed to orthorhombic coordination. Moreover, there were three bands at 772, 656, and 505 cm$^{-1}$ corresponding to the carbonyl group. At 400°C, the hydroxyl groups disappeared due to dehydration, while C=O and C-H bands were diminished. As the temperature increased to 800°C, bands due to Al-O stretching vibrations were seen at 750 and 580 cm$^{-1}$ that are characteristic of tetrahedral $AlO_4$ or $\eta$-$Al_2O_3$. When the temperature was 1050°C, characteristic bands of octahedral $AlO_6$ were observed at 780, 635, 567, 480, and 450 cm$^{-1}$ that are representative of $\alpha$-$Al_2O_3$. These results are consistent with those reported by Reyes-López et al. [11].

Figure 2 shows the $^{13}C$ MAS NMR spectrum of aluminum formate after heat treatment at 400°C. Initially, two types of peaks for carbonyl functional groups appeared at 170.33 and 171.39 ppm. After heating at 80°C, the peak at 170.33 decreased in intensity. Further heating at 240 and 270°C resulted in the reduction of these resonance bands, with subsequent disappearance at 400°C. The peak at 170 ppm corresponds to the carbonyl resonance of a carbon atom double-bonded to an oxygen atom in an acid or an ester. The changes seen in the spectra can be attributed to dehydration and complete loss of carbonyl groups.

The $^{27}Al$ MAS NMR spectrum of aluminum formate heated up to 1100°C (Figure 3) shows the disappearance of peaks at 0.60, −2.87, and− 26.29 ppm after heating at 270°C and emergence of new peaks at 72.03, 39.28, 12.21, and 7.79 ppm after heating over 400°C. As temperature increased, the hydroxyl and carbonyl groups were removed from the system. After heating at 400°C, a new peak corresponding to pentavalent aluminum ($Al^V$) appeared at 39.28 ppm. The conversion of aluminum formate to a transition alumina

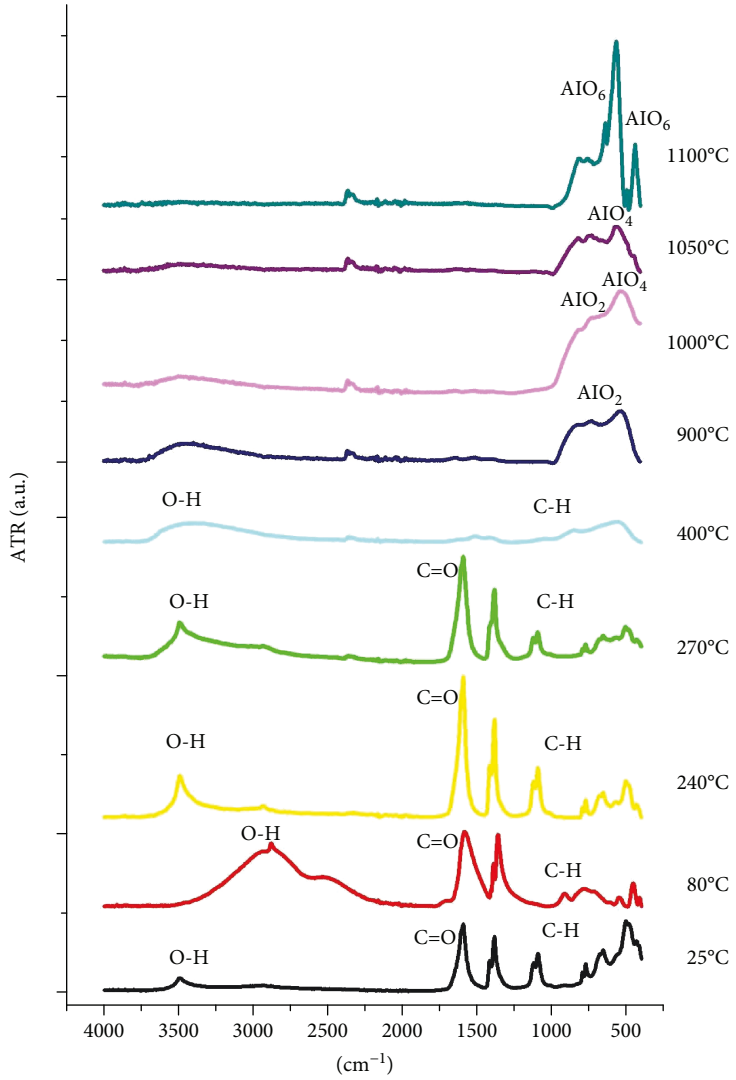


Figure 1: IR spectra of $Al(O_2CH)_3$ calcined at different temperatures.

phase with significant inherent disorder was indicated by the presence of five-coordinated aluminum. The five-coordinated aluminum usually appears in a mixture of alumina phases, such as $\gamma$ and $\delta$. However, the presence of $Al^{V}$ could not be determined by XRD, as the samples treated at 400°C did not show any crystalline structure. After heating at 900°C, a peak corresponding to tetrahedral aluminum ($Al^{V}$) appeared at 72.03 ppm. At 1100°C, two signals at 12.21 and 7.79 ppm associated with octahedral alumina ($Al^{VI}$) ($\alpha$-$Al_2O_3$) appeared.

Studies have shown that alumina in various stages of transition, represented by aluminum with coordination IV, V, and VI, can be found in different proportions in the same sample. The relative amount of each type of coordinated aluminum is reflected in the intensity of the peaks, which increases with temperature [12, 13]. These characterization results are supported by those of the X-ray diffraction analysis of the calcined powders previously reported [11].

After calcination at 1100°C, a fine white powder was obtained. The typical morphology of a spray-dried powder was observed in the SEM images, as shown in Figure 4(a). $\alpha$-$Al_2O_3$ powders were spherical and had a particle size distribution of $DP = 0.80 \pm 0.15\,\mu m$. Ring-shaped agglomerated nanoparticles with an average size of $20 \pm 7$ nm can be observed in Figure 4(b).

The surface area of the obtained alumina powders was also analyzed. The sample calcined at 600°C had a large surface area of 577 $m^2/g$. As the calcination temperature increased to 1000°C, the surface area drastically reduced to 180 $m^2/g$; at 1100°C, the surface area gradually decreased to 101 $m^2/g$. The changes in the surface area were caused by percentage increment of the $\alpha$-$Al_2O_3$ phase with the calcination temperature.

It is important to note that the size particle distribution is not uniform. We can appreciate the particle size in the nanometric and micrometric scales; however, this fact presupposes different reactivity degrees according to the particle size. It is well known that from the point of the nanometric scale, the reactivity of the particles is more significant in a small particle size [14]. In this sense, it is possible to appreciate also

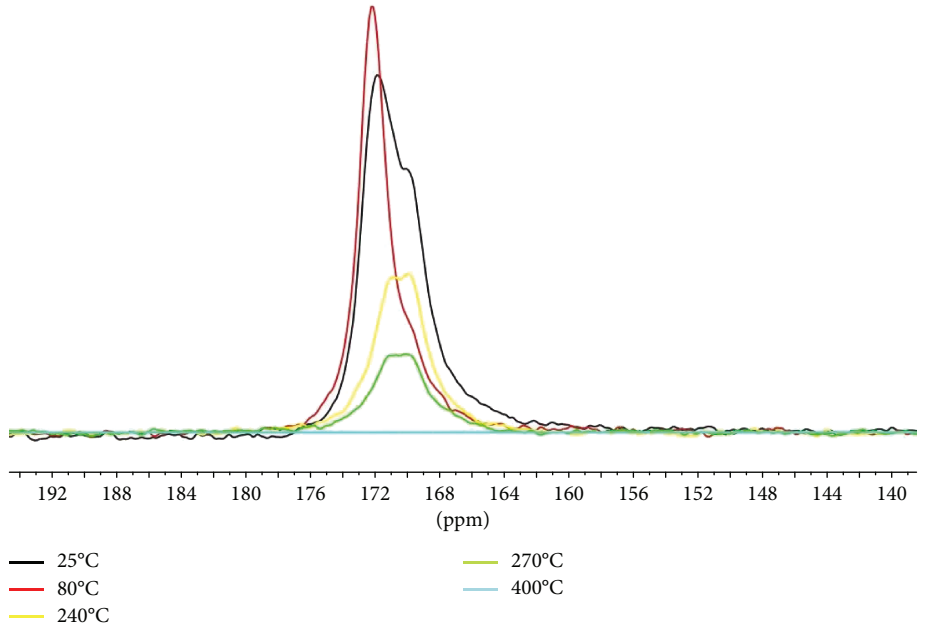


Figure 2: $^{13}$C MAS NMR spectra of aluminum formate after heat treatment at 25, 80, 240, 270, and 400°C.

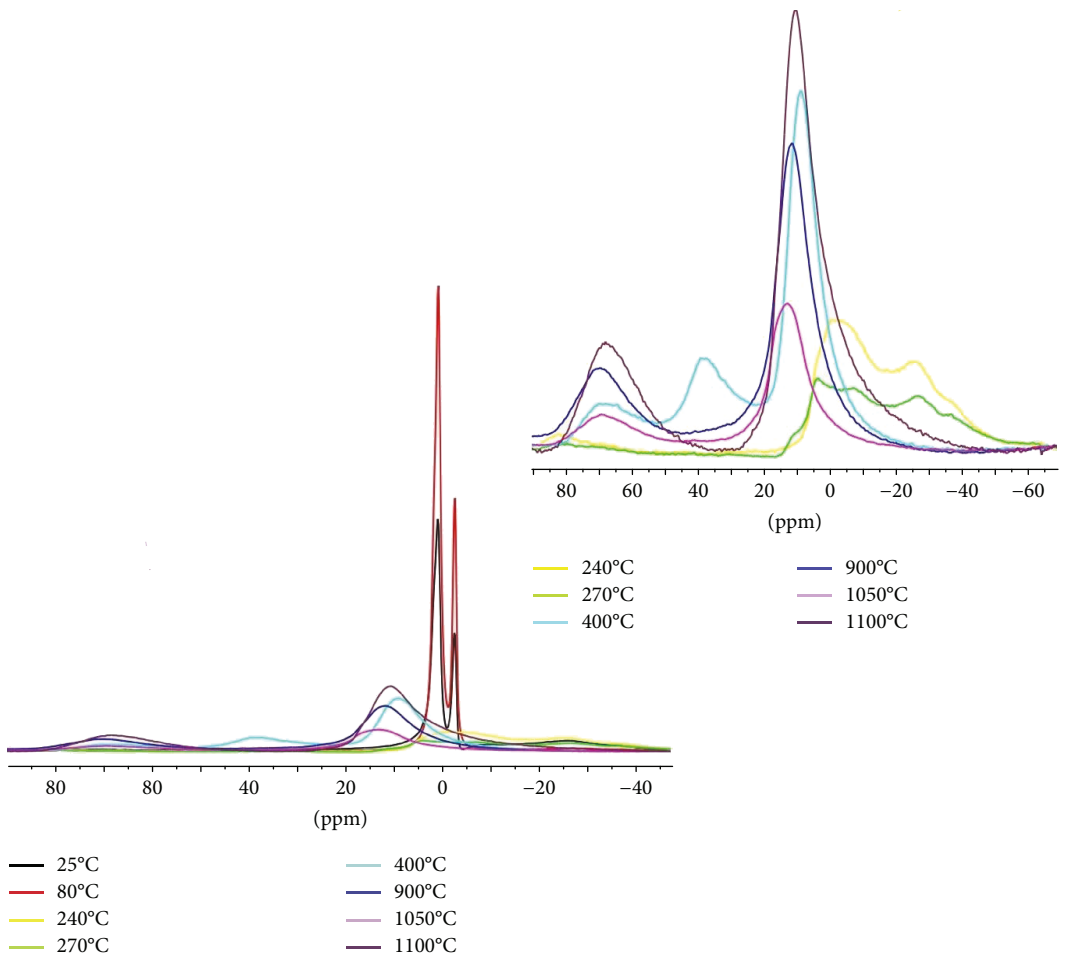


Figure 3: $^{27}$Al MAS NMR spectra of aluminum formate after heat treatment at 25, 80, 240, 270, 400, 900, 1050, and 1100°C.

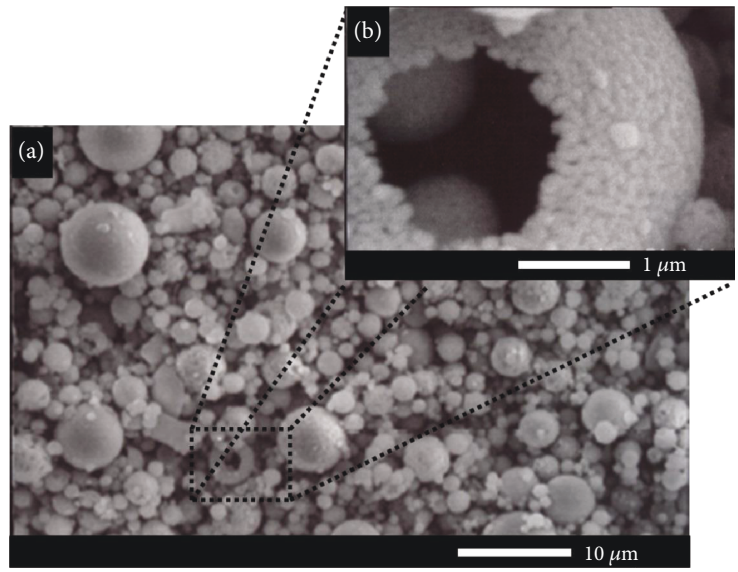


FIGURE 4: SEM images of $\alpha$-$Al_2O_3$ particles calcined at 1100°C. (a) 2000x and (b) 35,000x.

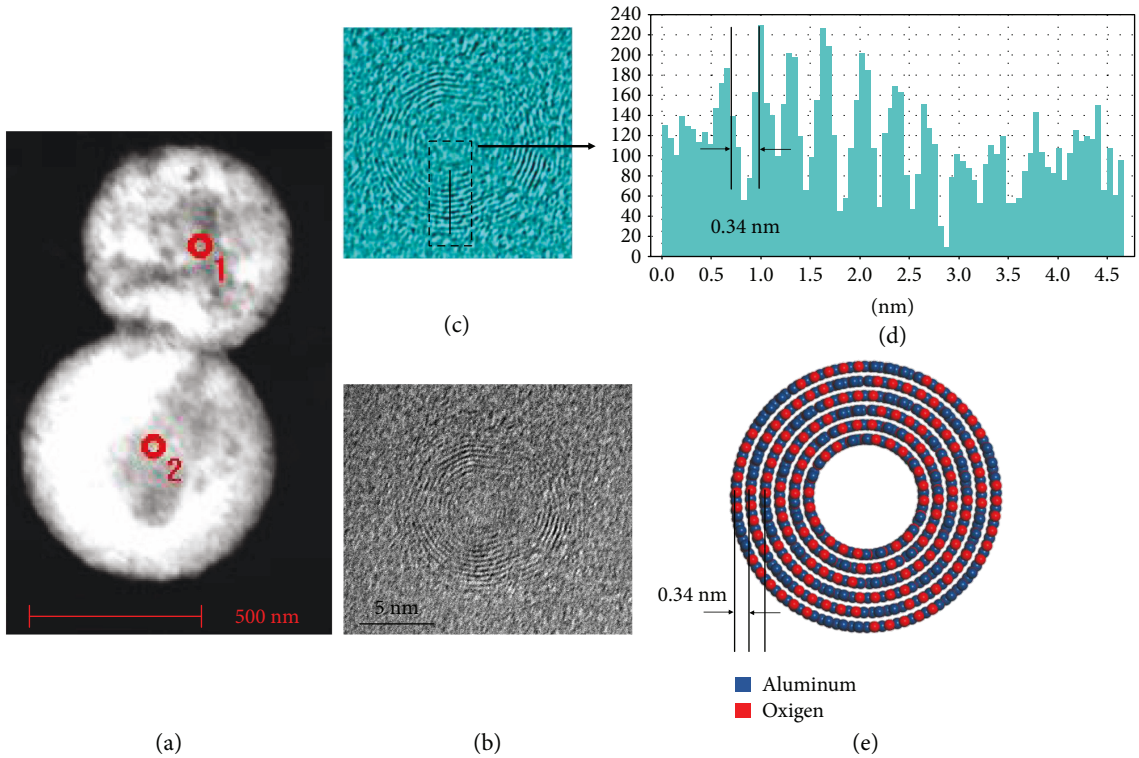


FIGURE 5: (a) STEM image of $\alpha$-$Al_2O_3$ at 1100°C, (b) HRTEM image of onion nanostructure, (c) HRTEM contrasted image, (d) image profile generated from the processed image, and (e) model of the onion nanostructure of $\alpha$-$Al_2O_3$.

nanostructure-like-type onion of $\alpha$-$Al_2O_3$ (Figure 4(b)). These structure probabilities were formed by the interaction of the most reactive $\alpha$-$Al_2O_3$ particles, several reports have described this growing mechanism [15–19]. The nano-onion structure observed is only present in the sample calcined at 1100°C; this fact can be explained from the thermodynamics point of view. In this sample, a major energy is employed during the formation process of $\alpha$-$Al_2O_3$; consequently, this energy favors the growing of nano-onion structures.

However, this finding should be considered a starting point for the synthesis of nanostructure-type onions,

considering that at calcination temperatures higher than 1100°C, it is possible to obtain a larger quantity of these structures.

In order to support the presence of the nano-onion structure observed, Figure 5(a) shows the STEM image of alumina spheres obtained at 1100°C. The contrast is associated with the atomic number of Al and O, allowing the identification of onion morphology. The nano-onions had an approximate size of $12.3 \pm 0.6$ nm. Nevertheless, the HRTEM image in Figure 5(b) confirms the formation of the nano-onion structure of $\alpha$-$Al_2O_3$. A better contrast of $\alpha$-$Al_2O_3$ nano-onion was obtained by employing the script Apply_-CLUT (color look-up table), useful for highlighting subtle intensity variations and making them more evident in color scale. The contrasted image is presented in Figure 5(c). Interplanar distances of the alumina atoms were obtained through an intensity profile generated from the contrasted image. The intensity profile in Figure 5(d) presents a distance of 0.341 nm associated with the (111) plane of $\alpha$-$Al_2O_3$. Figure 5(e) illustrates a model of the onion nanostructure of $\alpha$-$Al_2O_3$ that was prepared using the software QUANTA (Accelrys, San Diego, CA, USA).

Our results are supported by Karasev et al., who predicted the possible existence of $(Al_2O_3)_{1\text{-}5}$ and $Al_{20}O_{30}$ fullerene-like structures [20]. Alumina clusters can have stable onion-like structures. Sun et al. suggested that $(Al_2O_3)_n$ might be a good alternative for hydrogen storage according to its cage structure and electronic characteristics. If in the $(Al_2O_3)_n$ cage, each atom adsorbs one $H_2$ molecule, a hydrogen storage capacity can be achieved [21]. However, a systematic study of the obtained $\alpha$-$Al_2O_3$ structures is required to provide useful information for future research.

## 4. Conclusion

Carboxylates serve as useful precursors for $\alpha$-$Al_2O_3$ at relatively low temperatures (1100°C), thus simplifying the process and reducing costs. As shown by IR and NMR spectral data, heating at 400°C eliminates organic groups. $^{13}C$ MAS NMR spectra confirmed the disappearance of carbonyl groups when the precursor was heated at 400°C; this is in agreement with the results of IR analyses. The final transformation from $\eta$-$Al_2O_3$ to $\alpha$-$Al_2O_3$ occurred between 1000 and 1100°C. The solid-state NMR technique provides important structural information. $^{27}Al$ MAS NMR spectroscopy demonstrated the changes in aluminum coordination: at 400°C, pentavalent aluminum appeared, whereas at 800°C, the coordination changed to tetravalent aluminum. Finally, at 1100°C, octahedral aluminum appeared; this confirmed the formation of pure $\alpha$-$Al_2O_3$. As confirmed by HRTEM, the alumina nanoclusters can adopt stable nano-onion structures that can be potentially used as hydrogen storage material.

## Conflicts of Interest

The authors declare that there is no conflict of interest regarding the publication of this paper.

## Acknowledgments

The authors gratefully acknowledge the financial support from CONACYT and PROMEP. Simón Yobanny Reyes-López thanks Dr. Gerardo Gonzalez for the NMR analysis and Dra. Patricia Quintana-Owen for allowing access to LANNBIO CINVESTAV-Mérida, Yucatán, México.

## References

[1] E. Yalamaç, A. Trapani, and S. Akkurt, "Sintering and microstructural investigation of gamma–alpha alumina powders," *Engineering Science and Technology, an International Journal*, vol. 17, no. 1, pp. 2–7, 2014.

[2] J. Gangwar, B. K. Gupta, S. K. Tripathi, and A. K. Srivastava, "Phase dependent thermal and spectroscopic responses of $Al_2O_3$ nanostructures with different morphogenesis," *Nanoscale*, vol. 7, no. 32, pp. 13313–13344, 2015.

[3] J. Li and Y. Ye, "Densification and grain growth of $Al_2O_3$ nanoceramics during pressureless sintering," *Journal of the American Ceramic Society*, vol. 89, no. 1, pp. 139–143, 2006.

[4] Z. Zhao, X. Shen, H. Yao, J. Wang, J. Chen, and Z. Li, "Alumina nanofibers obtained via electrospinning of pseudo-boehmite sol/PVP solution," *Journal of Sol-Gel Science and Technology*, vol. 70, no. 1, pp. 72–80, 2014.

[5] K. Bodišová, P. Šajgalík, D. Galusek, and P. Švančárek, "Two-stage sintering of alumina with submicrometer grain size," *Journal of the American Ceramic Society*, vol. 90, no. 1, pp. 330–332, 2007.

[6] M. Vahtrus, M. Umalas, B. Polyakov et al., "Mechanical and structural characterizations of gamma- and alpha-alumina nanofibers," *Materials Characterization*, vol. 107, pp. 119–124, 2015.

[7] T. yan, X. Guo, X. Zhang, Z. Wang, and J. Shi, "Low temperature synthesis of nano alpha-alumina powder by two-step hydrolysis," *Materials Research Bulletin*, vol. 73, pp. 21–28, 2016.

[8] L. Xu, H. Song, and L. Chou, "Facile synthesis of nanocrystalline alpha-alumina at low temperature via an absolute ethanol sol–gel strategy," *Materials Chemistry and Physics*, vol. 132, no. 2-3, pp. 1071–1076, 2012.

[9] A. V. Galakhov, V. A. Zelenskii, N. A. Alad'ev, and L. V. Kovalenko, "$\alpha$-$Al_2O_3$ powders from amorphous alumina gel," *Inorganic Materials*, vol. 51, no. 3, pp. 201–205, 2015.

[10] J. Fang, I. Levchenko, X. P. Lu, D. Mariotti, and K. Ostrikov, "Hierarchical bi-dimensional alumina/palladium nanowire nano-architectures for hydrogen detection, storage and controlled release," *International Journal of Hydrogen Energy*, vol. 40, no. 18, pp. 6165–6172, 2015.

[11] S. Y. Reyes-López, R. Saucedo Acuña, R. López Juárez, and J. Serrato Rodríguez, "Analysis of the phase transformation of aluminum formate $Al(O_2CH)_3$ to $\alpha$-alumina by Raman and infrared spectroscopy," *Journal of Ceramic Processing Research*, vol. 14, no. 5, pp. 627–631, 2013.

[12] L. A. O'Dell, S. L. P. Savin, A. V. Chadwick, and M. E. Smith, "A $^{27}Al$ MAS NMR study of a sol–gel produced alumina: identification of the NMR parameters of the $\theta$-$Al_2O_3$ transition alumina phase," *Solid State Nuclear Magnetic Resonance*, vol. 31, no. 4, pp. 169–173, 2007.

[13] Á. d. J. Ruíz-Baltazar, S. Y. Reyes-López, D. Larrañaga, and R. Pérez, "Comparative study of Ag nanostructures: molecular

simulations, electrochemical behavior, and antibacterial effect," *Journal of Nanomaterials*, vol. 2016, Article ID 9372056, 9 pages, 2016.

[14] S. Shukrullah, N. M. Mohamed, Y. Khan, M. Y. Naz, A. Ghaffar, and I. Ahmad, "Effect of gas flowrate on nucleation mechanism of MWCNTs for a compound catalyst," *Journal of Nanomaterials*, vol. 2017, Article ID 3407352, 9 pages, 2017.

[15] T. Inmanee, P. Pinthong, and B. Jongsomjit, "Effect of calcination temperatures and Mo modification on nanocrystalline ($\gamma$-$\chi$)-$Al_2O_3$ catalysts for catalytic ethanol dehydration," *Journal of Nanomaterials*, vol. 2017, Article ID 5018384, 9 pages, 2017.

[16] L. Ren, X. Li, and S. Cui, "Synthesis of monolithic $Fe_2O_3$-$Al_2O_3$ composite aerogels via organic solvent sublimation drying," *Journal of Nanomaterials*, vol. 2016, Article ID 8135043, 6 pages, 2016.

[17] J. Li, X. Jiang, Z. Shao et al., "Microstructure and mechanical properties of multiphase strengthened Al/Si/$Al_2O_3$/$SiO_2$/MWCNTs nanocomposites sintered by in situ vacuum hot pressing," *Journal of Nanomaterials*, vol. 2015, Article ID 589754, 9 pages, 2015.

[18] Z. Wang, H. Hu, and X. Nie, "Preparation and characterization of highly flexible $Al_2O_3$/Al/$Al_2O_3$ hybrid composite," *Journal of Nanomaterials*, vol. 2015, Article ID 412071, 8 pages, 2015.

[19] J. H. Roque-Ruiz, E. A. Cabrera-Ontiveros, G. González-García, and S. Y. Reyes-López, "Thermal degradation of aluminum formate sol-gel; synthesis of α-alumina and characterization by $^1H$, $1^3C$ and $^{27}Al$ MAS NMR and XRD spectroscopy," *Results in Physics*, vol. 6, pp. 1096–1102, 2016.

[20] V. V. Karasev, A. A. Onischuk, O. G. Glotov et al., "Formation of charged aggregates of $Al_2O_3$ nanoparticles by combustion of aluminum droplets in air," *Combustion and Flame*, vol. 138, no. 1-2, pp. 40–54, 2004.

[21] J. Sun, W.-C. Lu, W. Zhang, L.-Z. Zhao, Z.-S. Li, and C.-C. Sun, "Theoretical study on ($Al_2O_3$)n ($n$ = 1–10 and 30) fullerenes and $H_2$ adsorption properties," *Inorganic Chemistry*, vol. 47, no. 7, pp. 2274–2279, 2008.